

Dynamic control of a reconfigurable stair-climbing mobility system

R. Morales†, J. Somolinos‡* and J. Cerrada§

†Department of Electrical, Electronics and Automation Engineering, University of Castilla-La Mancha, Albacete 02071, Spain

‡Department of Oceanic Systems, Universidad Politécnica de Madrid, Madrid 28040, Spain

§Department of Computer Systems and Software Engineering, Universidad Nacional de Educación a Distancia (UNED), Madrid 28040, Spain

(Accepted April 20, 2012. First published online: May 24, 2012)

SUMMARY

Electric-powered wheelchairs improve the mobility of people with physical disabilities, but the problem to deal with certain architectural barriers has not been resolved satisfactorily. In order to solve this problem, a stair-climbing mobility system (SCMS) was developed. This paper presents a practical dynamic control system that allows the SCMS to exhibit a successful climbing process when faced with typical architectural barriers such as curbs, ramps, or staircases. The implemented control system depicts high simplicity, computational efficiency, and the possibility of an easy implementation in a microprocessor-/microcontroller-based system. Finally, experiments are included to support theoretical results.

KEYWORDS: Electric-powered wheelchairs; Stair-climbing devices; Dynamic modeling; Dynamic control; Mechatronics.

List of Symbols

Symbol	Description
l_i [m]	Lengths of the bars of the mechanical system.
θ_1, θ_2 (rad)	Front and rear angles of joints of a chair structure.
$\dot{\theta}_1, \dot{\theta}_2$ (rad/s)	Front and rear angular velocities of joints of a chair structure.
$\ddot{\theta}_1, \ddot{\theta}_2$ (rad/s ²)	Front and rear angular accelerations of joints of a chair structure.
$\mathbf{f}(\theta_4), \mathbf{f}(\theta_3)$ (m)	Position of axles of front and rear wheels.
z_1, z_2 (m)	Instantaneous length of front and rear racks.
\dot{z}_1, \dot{z}_2 (m/s)	Velocity of front and rear racks.
\ddot{z}_1, \ddot{z}_2 (m/s ²)	Acceleration of front and rear racks.
$\mathbf{P}_{C1}, \mathbf{P}_{C2}$ (m)	Position of contact points of racks.

\mathbf{P}_g (m)	Center of mass position.
γ (rad)	Inclination of chair seat.
$\dot{\gamma}$ (rad/s)	Angular velocity of chair seat.
$\ddot{\gamma}$ (rad/s ²)	Angular acceleration of chair seat.
β_1, β_2 (rad)	Slopes of front and rear racks.
$\mathbf{r} = [r_1, r_2]^T$ (rad)	Vector of generalized coordinate variables.
$\dot{\mathbf{r}} = [\dot{r}_1, \dot{r}_2]^T$ (rad/s)	Angular velocity of generalized coordinate variables.
$\ddot{\mathbf{r}} = [\ddot{r}_1, \ddot{r}_2]^T$ (rad/s ²)	Angular acceleration of generalized coordinate variables.
$\boldsymbol{\tau} = [\tau_1, \tau_2]^T$ (N · m)	Torques exerted in the center of gravity of the mechanism.

1. Introduction

Independent mobility is crucial for the development of physical, cognitive, communicative, and social skills.¹ The development of technology that facilitates the rehabilitation of people with severe or multiple handicaps in every day life is desirable. Conventional Electric-Powered Wheelchairs (EPWs) are the principal means of mobility for a large percentage of people with physical disabilities, and it is unquestionable that EPWs greatly improve the mobility of these people.² Nevertheless, architectural barriers still exist in many cities and buildings, and it is expensive and time-consuming, if not impossible, to eliminate all such barriers. New tendencies have arisen with the development of stair-climbing mobility systems (SCMSs), which are capable of negotiating architectural barriers in order to provide people with walking difficulties with more autonomy and to reduce the amount of labor-intensive manhandling of patients by care workers.³ SCMSs are currently rated by the Food and Drug Administration (FDA) as “class III” high-risk devices, defined as “life-sustaining or life-supporting, implanted in the body, or present an unreasonable risk of illness or injury.”⁴ The provision of acceptable stability at all times for a SCMS is therefore essential for safety during stair climbing, and, additionally, a constant seat angle is usually desired. Stair-climbing devices are usually of three types: a crawler type, a wheel type, and a legged type. The crawler-type⁵ devices shows high terrain adaptivity and robustness but they present

* Corresponding author. E-mail: joseandres.somolinos@upm.es

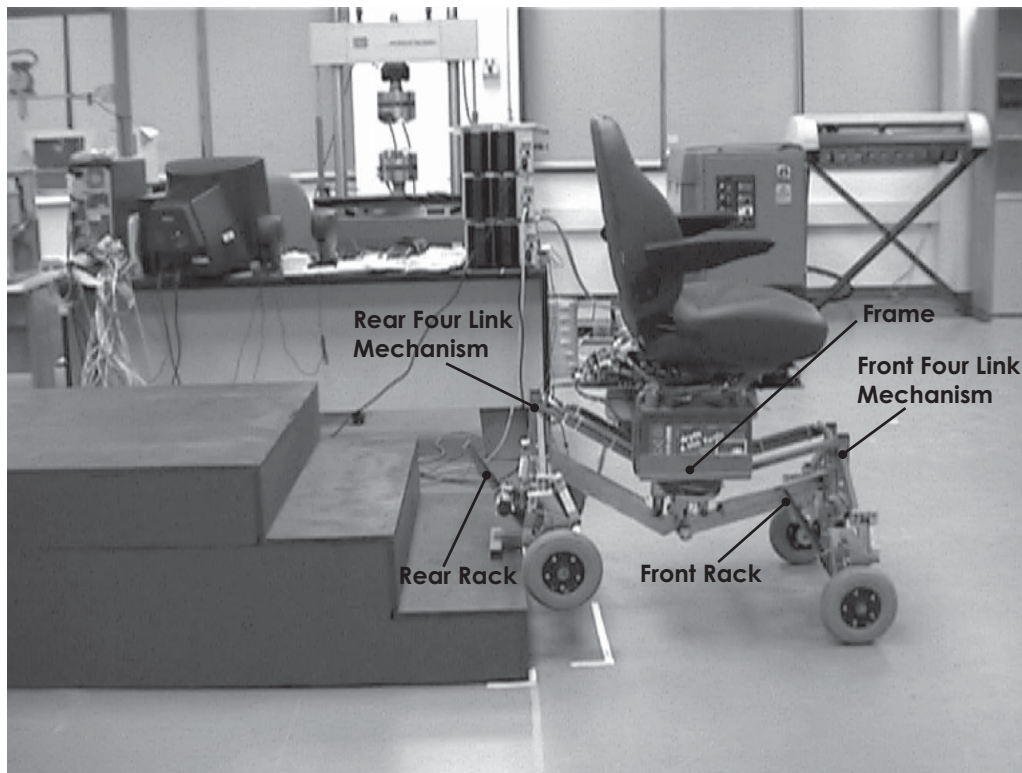


Fig. 1. Designed prototype.

low locomotion efficiency in barrier-free environments. In the wheeled-type devices, the energy efficiency when moving on flat terrain is higher than in other types but has problems when there appear architectural barriers. A commonly used solution is based on several wheels arranged in a rotating link (clusters).³ Its drawback is that it relies on complicated dynamic controllers to maintain the upright position and there are motion phases during climbing or descent obstacles that the system is standing on just two wheels with a common axis. Alternative designs that use clusters have good rolling efficiency and conceptual simplicity but present a high actuating cluster torque and a high number of wheels that must be driven and braked.⁶ The legged-type devices have the highest adaptivity to rough terrain⁷ but have the following disadvantages: load, weight, energy efficiency, and speed of motion. Then, the best way to solve architectural barriers is by means of mixed systems. These devices combine legs (high terrain adaptability) and wheels (high efficiency and payload capability),⁸ and some models have been designed with the objective of providing mobility to people with physical disabilities but present problems in the step-climbing process as a result of a large variation in the chair inclination angle.⁹

There is a limited amount of literature concerning the modeling of SCMSs, and one of the reasons for this is that these models are not required for a simple control law commonly adopted by commercial EPWs. In the case of stair-climbing devices the definition of a mathematical model is extremely important because it will be necessary to achieve advanced controllers that improve the stair-climbing process. Some authors have proposed simplified models based on a kinematic model¹⁰ and its corresponding kinematic feedback control laws.¹¹ These control schemes are justified because

the prototype moves at low speeds, high precision is not necessary, and the control law is easier to implement (reduction in the amount of computation resources, cost, and sensorial system). The most important limitation is that kinematic control is not robust to perturbations in the system, error modeling, and environmental uncertainties.¹² The definition of the dynamics model of the stair-climbing device and the design of a control law based on its dynamics model will help to reduce the effect of these error sources.¹³ In order to achieve a successful stair-climbing process, the SCMS presented in this paper (Fig. 1) must change its configuration (see refs. [14 and 15] to obtain a detailed description about the mechanical system of the prototype). This implies that the dynamics model must be defined by including all the possible configurations. On the other hand, the control law based on the dynamics model must include an additional device in charge of the selection of appropriate configuration. In this work, based on the dynamics model of the SCMS and taking into account all its possible configurations, it has been developed by the necessary control law to obtain a successful behavior when the prototype confronts architectural barriers such as curbs, ramps, or staircases. The proposed control law is divided into two different modules. First, we have created a behavior diagram that selects correct configuration to overcome a particular obstacle; and second, to maintain the passenger comfort, reduce the perturbation effects, and eliminate the possibility of turning over, a control law based on a proportional-derivative (PD) controller with nonlinear compensation of gravitational terms has been included. The stability analysis of this control scheme is analyzed by using the Lyapunov procedure as in refs. [16] and [17]. These kind of control schemes have a widespread use in commercial

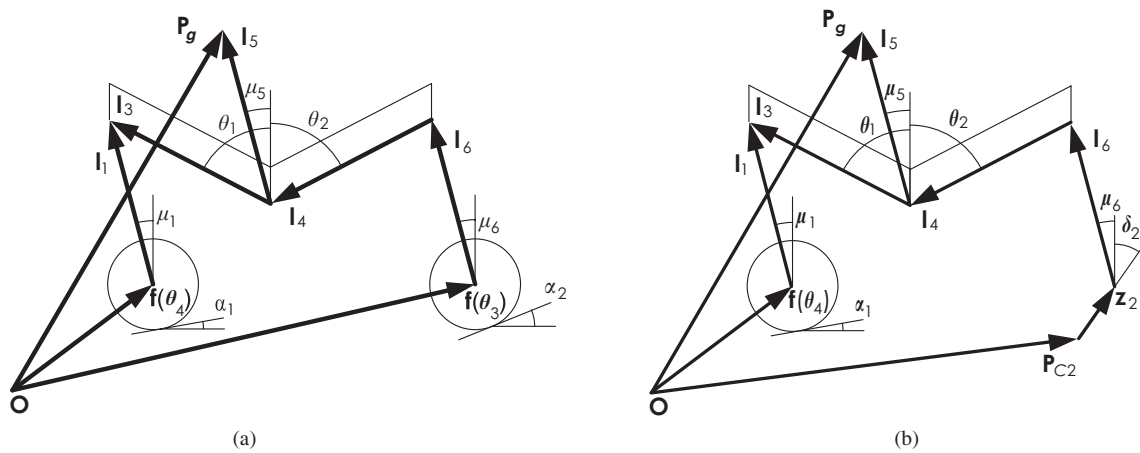


Fig. 2. General kinematic scheme when the SCMS is supported (a) on four wheels; (b) on rear rack and front wheels.

industrial robots but they have seldom been used on SCMSs. Finally, the whole scheme has been experimentally tested with highly encouraging results as the prototype ascends a staircase.

The paper is organized as follows: Section 2 is devoted to derive the direct kinematic model of SCMS taking into account all the different configurations of the system during a stair-climbing/descent process. Section 3 proposes a dynamics model for SCMS in generalized coordinate variables. Section 4 describes relations between generalized articular variables and system variables in all the possible configurations of SCMS. Section 5 explains the adopted solution for the control of the system. Section 6 presents the experimental results obtained to validate the proposed control algorithm, and finally, Section 7 is devoted to the conclusions of the paper as well as proposals for future work.

2. Direct Kinematic Model

The kinematic model¹⁵ and the trajectory generation¹⁸ allow full motion of the degrees of freedom of the whole system, and can be adapted to a continuous smooth profile or a discontinuous profile consisting of a flat floor and a staircase. Furthermore, the choice of an appropriate movement strategy influences the verticality of the chair frame, the passenger comfort (the SCMS will usually carry a passenger with physical disabilities), and the power consumption. In this section, the direct kinematic model presented in ref [18] is described briefly, since this will clarify the relation between the articular variables of the dynamics model presented in Section 3 and the system variables in all the possible configurations of the prototype illustrated in Section 4. The use of a complex notation greatly facilitates any dealings with kinematic models for SCMS, since the expression of rotations is simplified, leading to more compact equations and a simplification of computer resources and control. The horizontal variable (defined as $Re[\mathbf{z}]$) and the vertical variable (defined as $Im[\mathbf{z}]$) are the real and the imaginary components of a complex number. In the direct kinematic model, there are the angles of the joints of the chair structure (θ_1 and θ_2) and the position of axles of front and rear wheels in the complex plane (given by $\mathbf{f}(\theta_4)$ and $\mathbf{f}(\theta_3)$, respectively, and θ_3 is the turn angle of the rear wheels) or the instantaneous

lengths of the racks (z_1 and z_2) and their corresponding contact points (\mathbf{P}_{C1} and \mathbf{P}_{C2}), depending on the configuration. These data are used to obtain the center of mass position (\mathbf{P}_g) and the inclination of the SCMS seat (γ). The direct kinematic model for each of the different configurations of SCMS is now briefly presented.

2.1. SCMS supported on four wheels

In this configuration, the SCMS is supported on four wheels (see Fig. 2(a)). It is assumed that the rear and front axles are rolling on a flat terrain and the angles μ_i are defined to find geometrical connection between vectors comprising the general kinematic scheme. Following are the initial expressions that define the current position of SCMS:

$$\mathbf{P}_g = \mathbf{f}(\theta_3) + l_6 e^{j(\gamma + \frac{\pi}{2} + \mu_6)} + l_4 e^{j(\gamma + \frac{3\pi}{2} - \theta_2)} + l_5 e^{j(\gamma + \frac{\pi}{2} + \mu_5)}, \tag{1}$$

$$\mathbf{P}_g = \mathbf{f}(\theta_4) + l_1 e^{j(\gamma + \frac{\pi}{2} + \mu_1)} - l_3 e^{j(\gamma + \frac{\pi}{2} + \theta_1)} + l_5 e^{j(\gamma + \frac{\pi}{2} + \mu_5)}, \tag{2}$$

where, using the notation depicted in ref. [18], l_1 and l_3 are the lengths that correspond with the front axle, l_4 and l_6 are the lengths that correspond with the rear axle, and l_5 is the length from the frame to the center of mass, \mathbf{P}_g .

2.2. SCMS supported on the rear rack and the front wheels

In this configuration, the SCMS is supported on the rear rack and the front wheels (see Fig. 2(b)). It is assumed that the front axle is rolling on a flat terrain and the rear rack is moving with a slope of $\beta_2 = \frac{\pi}{2} - \delta_2$. The initial expressions that define the current position of the SCMS are shown here:

$$\mathbf{P}_g = \mathbf{f}(\theta_4) + l_1 e^{j(\gamma + \frac{\pi}{2} + \mu_1)} - l_3 e^{j(\gamma + \frac{\pi}{2} + \theta_1)} + l_5 e^{j(\gamma + \frac{\pi}{2} + \mu_5)}, \tag{3}$$

$$\mathbf{P}_g = \mathbf{P}_{C2} + z_2 e^{j(\gamma + \frac{\pi}{2} - \delta_2)} + l_6 e^{j(\gamma + \frac{\pi}{2} + \mu_6)} + l_4 e^{j(\gamma + \frac{3\pi}{2} - \theta_2)} + l_5 e^{j(\gamma + \frac{\pi}{2} + \mu_5)}, \tag{4}$$

where δ_2 is the inclination angle of the rear rack, which composes the rear climbing mechanism.

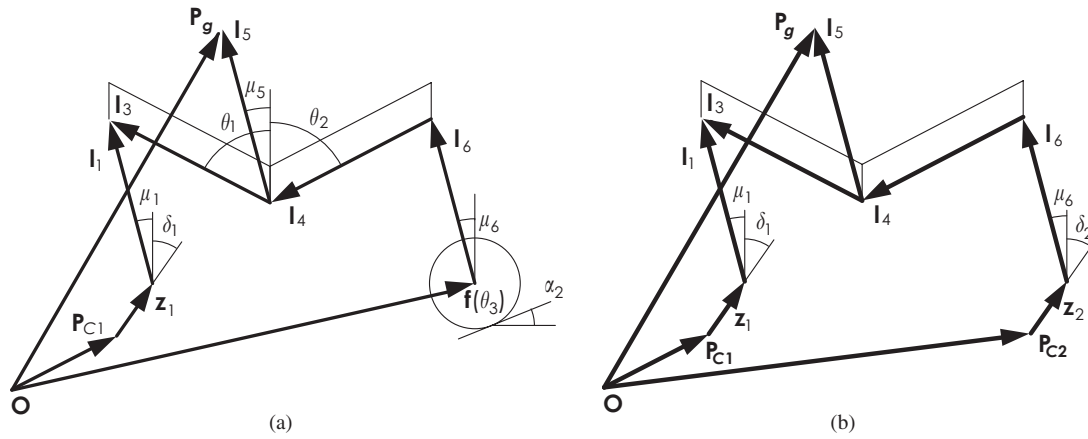


Fig. 3. General kinematic scheme when the SCMS is supported (a) on front rack and rear wheels, (b) on two racks.

2.3. SCMS supported on the front rack and the rear wheels

In this configuration, the SCMS is supported on the front rack and the rear wheels (see Fig. 3(a)). It is assumed that the rear axle is rolling on flat terrain and the front rack is moving with a slope of $\beta_1 = \frac{\pi}{2} - \delta_1$. Following are the initial expressions that define the current position of the SCMS:

$$P_g = f(\theta_3) + l_6 e^{j(\gamma + \frac{\pi}{2} + \mu_6)} + l_4 e^{j(\gamma + \frac{3\pi}{2} - \theta_2)} + l_5 e^{j(\gamma + \frac{\pi}{2} + \mu_5)}, \tag{5}$$

$$P_g = P_{C1} + z_1 e^{j(\gamma + \frac{\pi}{2} - \delta_1)} + l_1 e^{j(\gamma + \frac{\pi}{2} + \mu_1)} - l_3 e^{j(\gamma + \frac{\pi}{2} + \theta_1)} + l_5 e^{j(\gamma + \frac{\pi}{2} + \mu_5)}, \tag{6}$$

where δ_1 is the inclination angle of the front rack, which composes the front climbing mechanism.

2.4. SCMS supported on two racks

In this configuration, the SCMS is supported on two racks (see Fig. 3(b)). The rear and front racks are moving with the corresponding slopes $\beta_1 = \frac{\pi}{2} - \delta_1$ and $\beta_2 = \frac{\pi}{2} - \delta_2$. The initial expressions that define the current position of the SCMS are shown here:

$$P_g = P_{C2} + z_2 e^{j(\gamma + \frac{\pi}{2} - \delta_2)} + l_6 e^{j(\gamma + \frac{\pi}{2} + \mu_6)} + l_4 e^{j(\gamma + \frac{3\pi}{2} - \theta_2)} + l_5 e^{j(\gamma + \frac{\pi}{2} + \mu_5)}, \tag{7}$$

$$P_g = P_{C1} + z_1 e^{j(\gamma + \frac{\pi}{2} - \delta_1)} + l_1 e^{j(\gamma + \frac{\pi}{2} + \mu_1)} - l_3 e^{j(\gamma + \frac{\pi}{2} + \theta_1)} + l_5 e^{j(\gamma + \frac{\pi}{2} + \mu_5)}. \tag{8}$$

3. Dynamics Model

The derivation of the dynamics model of a SCMS plays an important role in the simulation of motion, the mechanism structure analysis, and the design of control algorithms. The dynamics model chosen must be precise enough to describe different behaviors of the mechanism and simple enough to include it in the control law.¹⁹ In our case, the dynamics model of the SCMS expressed in terms of generalized coordinates is the same for all prototype configurations. However, the relation between the generalized coordinates

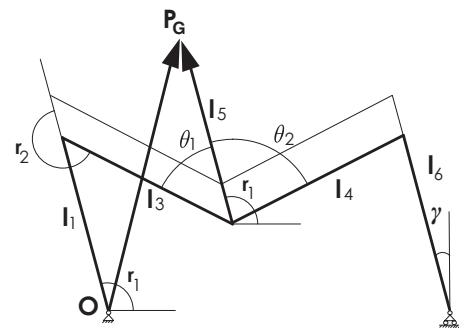


Fig. 4. Definition of generalized coordinate variables of SCMS.

and the system coordinates in each particular configuration are different and this must be considered in order to adapt different equations to different system configurations.

The first step consists of obtaining expressions of forces that appear in the mechanism in terms of the generalized coordinate variable, $r = [r_1, r_2]^T$. Figure 4 shows the notation used to obtain the dynamics model. With this notation, the position of the end effector is given by the following result:

$$\overline{OP_g} = \begin{bmatrix} x \\ y \end{bmatrix} = \begin{bmatrix} (l_1 + l_5) C_{r_1} + l_3 C_{(r_1+r_2)} \\ (l_1 + l_5) S_{r_1} + l_3 S_{(r_1+r_2)} \end{bmatrix}, \tag{9}$$

where $S_{r_i} = \sin r_i$ and $C_{r_i} = \cos r_i$. The expressions for velocities in the articular coordinate frame can be obtained by differentiating Eq. (9),

$$\dot{\overline{OP_g}} = \begin{bmatrix} \dot{x} \\ \dot{y} \end{bmatrix} = \begin{bmatrix} -(l_1 + l_5) S_{r_1} \dot{r}_1 - l_3 S_{(r_1+r_2)} (\dot{r}_1 + \dot{r}_2) \\ (l_1 + l_5) C_{r_1} \dot{r}_1 + l_3 C_{(r_1+r_2)} (\dot{r}_1 + \dot{r}_2) \end{bmatrix}. \tag{10}$$

Using the same procedure, the expressions for accelerations in the articular coordinate frame can be obtained by differentiating Eq. (10),

$$\ddot{\overline{OP_g}} = [\ddot{x} \ \ddot{y}]^T, \tag{11}$$

where

$$\ddot{x} = -(l_1 + l_5)[C_{r_1}\dot{r}_1^2 + S_{r_1}\ddot{r}_1] - l_3[C_{(r_1+r_2)}(\dot{r}_1 + \dot{r}_2)^2 + S_{(r_1+r_2)}(\ddot{r}_1 + \ddot{r}_2)], \tag{12}$$

$$\ddot{y} = (l_1 + l_5)[-S_{r_1}\dot{r}_1^2 + C_{r_1}\ddot{r}_1] + l_3[-S_{(r_1+r_2)}(\dot{r}_1 + \dot{r}_2)^2 + C_{(r_1+r_2)}(\ddot{r}_1 + \ddot{r}_2)]. \tag{13}$$

The forces that appear in the center of mass \mathbf{P}_g of the mechanism, \mathbf{F}_M , are achieved from expression (11), and are given by the following result,

$$\mathbf{F}_M = m \cdot \overline{\ddot{\mathbf{OP}}_g} = m \cdot [\ddot{x} \ \ddot{y}]^T, \tag{14}$$

where m is the mass of the whole system (passenger + prototype). It is important to note that the mass of the system does not change during the process of movement and it can be measured with a sensor mounted on the prototype. Moreover, taking into account the mechanical stability demonstrated in ref. [18], the position of center of mass of the prototype barely changes during the climbing/descending process (it is assumed that since the climbing/descending process is a delicate task, the user will not make abrupt movements).

The gravity is defined as $\mathbf{g} = [0, -g]^T$. Then the forces owing to the gravity effect are obtained as

$$\mathbf{F}_{G_{xy}} = m[0 \ -g]^T. \tag{15}$$

If the results of the forces given by expressions (14) and (15) are grouped, and the Newton's Second Law is applied, the generalized forces exerted in the center of mass of the mechanism, \mathbf{F}_{P_g} , are given by the following expressions:

$$\mathbf{F}_{P_g} = m \cdot \left[\mathbf{A}_1 \cdot \begin{bmatrix} \dot{r}_1 \\ \dot{r}_2 \end{bmatrix} + \mathbf{A}_2 \cdot \begin{bmatrix} \dot{r}_1 \\ \dot{r}_2 \end{bmatrix} + \begin{bmatrix} 0 \\ g \end{bmatrix} \right], \tag{16}$$

$$\mathbf{A}_1 = \begin{bmatrix} -[(l_1 + l_5)S_{r_1} + l_3S_{(r_1+r_2)}] & -l_3S_{(r_1+r_2)} \\ [(l_1 + l_5)C_{r_1} + l_3C_{(r_1+r_2)}] & l_3C_{(r_1+r_2)} \end{bmatrix},$$

$$\mathbf{A}_2 = \begin{bmatrix} -[(l_1 + l_5)C_{r_1} + l_3C_{(r_1+r_2)}]\dot{r}_1 & -l_3C_{(r_1+r_2)}(2\dot{r}_1 + \dot{r}_2) \\ -[(l_1 + l_5)S_{r_1} + l_3S_{(r_1+r_2)}]\dot{r}_1 & -l_3S_{(r_1+r_2)}(2\dot{r}_1 + \dot{r}_2) \end{bmatrix}.$$

It is well known that under quasi-static conditions, the relation between the torques exerted in the joints and the forces and torques exerted in the center of gravity of the mechanism are related by the following expression:

$$\boldsymbol{\tau} = \mathbf{J}^T(\mathbf{r})\mathbf{F}_{P_g}, \tag{17}$$

where the Jacobian, $\mathbf{J}(\mathbf{r})$, is obtained directly from Eq. (9) as follows:

$$\mathbf{J}(\mathbf{r}) = \begin{bmatrix} \frac{\partial x}{\partial r_1} & \frac{\partial x}{\partial r_2} \\ \frac{\partial y}{\partial r_1} & \frac{\partial y}{\partial r_2} \end{bmatrix} = \begin{bmatrix} -[(l_1 + l_5)S_{r_1} + l_3S_{(r_1+r_2)}] & -l_3S_{(r_1+r_2)} \\ (l_1 + l_5)C_{r_1} + l_3C_{(r_1+r_2)} & l_3C_{(r_1+r_2)} \end{bmatrix}. \tag{18}$$

Upon substituting Eq. (18) in Eq. (17), and after certain algebraic manipulations, the following dynamics model for the SCMS is obtained:

$$\boldsymbol{\tau} = \mathbf{B}(\mathbf{r})\ddot{\mathbf{r}} + \mathbf{C}(\mathbf{r}, \dot{\mathbf{r}})\dot{\mathbf{r}} + \mathbf{G}(\mathbf{r}), \tag{19}$$

where the values of the matrices $\mathbf{B}(\mathbf{r})$, $\mathbf{C}(\mathbf{r}, \dot{\mathbf{r}})$, and $\mathbf{G}(\mathbf{r})$ are given by the following expressions:

$$\mathbf{B}(\mathbf{r}) = m \begin{bmatrix} (l_1 + l_5)^2 + l_3^2 + 2l_3(l_1 + l_5)C_{r_2} & l_3^2 + l_3(l_1 + l_5)C_{r_2} \\ l_3^2 + l_3(l_1 + l_5)C_{r_2} & l_3^2 \end{bmatrix}, \tag{20}$$

$$\mathbf{C}(\mathbf{r}, \dot{\mathbf{r}}) = m \begin{bmatrix} 0 & -l_3(l_1 + l_5)S_{r_2}(2\dot{r}_1 + \dot{r}_2) \\ l_3(l_1 + l_5)S_{r_2}\dot{r}_1 & 0 \end{bmatrix}, \tag{21}$$

$$\mathbf{G}(\mathbf{r}) = mg \begin{bmatrix} (l_1 + l_5)C_{r_1} + l_3C_{(r_1+r_2)} \\ l_3C_{(r_1+r_2)} \end{bmatrix}. \tag{22}$$

The computation of articular variables and their corresponding derivatives ($\mathbf{r} = [r_1, r_2]^T$, $\dot{\mathbf{r}} = [\dot{r}_1, \dot{r}_2]^T$, and $\ddot{\mathbf{r}} = [\ddot{r}_1, \ddot{r}_2]^T$) expressed in terms of the system variables ($\mathbf{q} = [\theta_1, \theta_2, \theta_3, z_1, z_2]^T$, $\dot{\mathbf{q}} = [\dot{\theta}_1, \dot{\theta}_2, \dot{\theta}_3, \dot{z}_1, \dot{z}_2]^T$, and $\ddot{\mathbf{q}} = [\ddot{\theta}_1, \ddot{\theta}_2, \ddot{\theta}_3, \ddot{z}_1, \ddot{z}_2]^T$) will depend on the particular configuration of the mechanism. It is therefore necessary to find a relation between the articular variables and the system variables for all the possible configurations and to use the model given by Eq. (19) in order to obtain a new model as a function of \mathbf{q} rather than \mathbf{r} , i.e.,

$$\boldsymbol{\tau} = \mathbf{B}(\mathbf{q})\ddot{\mathbf{q}} + \mathbf{C}(\mathbf{q}, \dot{\mathbf{q}})\dot{\mathbf{q}} + \mathbf{G}(\mathbf{q}). \tag{23}$$

4. Relation between articular variables and system variables in all the possible configurations

By using the dynamics model defined in Section 3, the special system geometry ($l_1 = l_6$, $l_3 = l_4$, and $\mu_1 = \mu_6 = \mu_5 = 0$) and taking advantage of the fact that in the positioning mechanism the frames of the front and rear axles do not rotate with regard to the main frame, the following relations are obtained (see Fig. 3):

$$r_1 = \frac{\pi}{2} + \gamma; \quad r_2 = \pi + \theta_1. \tag{24}$$

In the same manner, by differentiating the above expressions, following are the relations for velocities and accelerations:

$$\dot{r}_1 = \dot{\gamma}; \quad \dot{r}_2 = \dot{\theta}_1 \quad \ddot{r}_1 = \dot{\gamma}; \quad \ddot{r}_2 = \ddot{\theta}_1. \quad (25)$$

This system property makes it necessary to obtain mathematical relations between articular variables and control variables of the actuated degrees of freedom of SCMS for all possible configurations. This will be dealt with in the following subsections.

4.1. Relation between articular variables and control variables when the SCMS is supported on four wheels

Expressions (1) and (2) define the current position of this SCMS configuration. Computing the difference of expressions (1) and (2), and defining the complex variable $\mathbf{f}(\theta_3) - \mathbf{f}(\theta_4) = |\mathbf{f}(\theta_3) - \mathbf{f}(\theta_4)|e^{j\Delta_1}$ yields

$$|\mathbf{f}(\theta_3) - \mathbf{f}(\theta_4)| e^{j\Delta_1} + l_3 \left(e^{j(\gamma + \frac{\pi}{2} + \theta_1)} + e^{j(\gamma + \frac{3\pi}{2} - \theta_2)} \right) = \mathbf{0}. \quad (26)$$

If both sides of expression (26) are multiplied by the magnitude $e^{-j(\gamma + \frac{\pi}{2} + \theta_1)}$ and certain algebraic manipulations are carried out, the following expression is reached:

$$|\mathbf{f}(\theta_3) - \mathbf{f}(\theta_4)| e^{j(\Delta_1 - \gamma + \frac{\pi}{2} - \theta_1)} = l_3 (1 + e^{j(\pi - \theta_1 - \theta_2)}). \quad (27)$$

The unknown variables are Δ_1 , $|\mathbf{f}(\theta_3) - \mathbf{f}(\theta_4)|$, and γ . Moreover, although the complex magnitude $\mathbf{f}(\theta_3) - \mathbf{f}(\theta_4)$ is not known, it can be seen that its imaginary part, $(Im[\mathbf{f}(\theta_3) - \mathbf{f}(\theta_4)])$, has a known constant value. Taking into account the previous considerations and separating expression (27) into its corresponding equations of modulus and phases, the following results are obtained (expressed in the order of calculation):

$$|\mathbf{f}(\theta_3) - \mathbf{f}(\theta_4)| = l_3 |1 + e^{j(\pi - \theta_1 - \theta_2)}|, \quad (28)$$

$$\Delta_1 = \arcsin \left(\frac{Im[\mathbf{f}(\theta_3) - \mathbf{f}(\theta_4)]}{|\mathbf{f}(\theta_3) - \mathbf{f}(\theta_4)|} \right), \quad (29)$$

$$\gamma = \Delta_1 + \frac{\pi}{2} - \theta_1 - \text{phase} [(1 + e^{j(\pi - \theta_1 - \theta_2)})]. \quad (30)$$

Considering the geometrical relations and taking the imaginary part, the values of variables $\dot{\gamma}$ and $\ddot{\gamma}$ are reached by using expressions (1) and (2). The following result is yielded:

$$Im[\mathbf{f}(\theta_4) - \mathbf{f}(\theta_3)] = l_3 \left[S_{(\gamma + \frac{3\pi}{2} - \theta_2)} + S_{(\gamma + \frac{\pi}{2} + \theta_1)} \right]. \quad (31)$$

Upon differentiating Eq. (31) and after certain algebraic manipulations, the following expression is obtained for $\dot{\gamma}$:

$$\dot{\gamma} = \frac{-S_{(\theta_1 + \gamma)}\dot{\theta}_1 + S_{(\theta_2 - \gamma)}\dot{\theta}_2}{S_{(\theta_1 + \gamma)} + S_{(\theta_2 - \gamma)}} \quad (32)$$

Finally, by differentiating Eq. (32), and after certain algebraic manipulations, the expression for $\ddot{\gamma}$ is written as:

$$\ddot{\gamma} = \frac{num_1}{den_1}, \quad (33)$$

where

$$num_1 = -C_{(\theta_1 + \gamma)}(\dot{\theta}_1 + \dot{\gamma})^2 + C_{(\theta_2 - \gamma)}(\dot{\theta}_2 - \dot{\gamma})^2 - S_{(\theta_1 + \gamma)}\ddot{\theta}_1 + S_{(\theta_2 - \gamma)}\ddot{\theta}_2, \quad (34)$$

$$den_1 = S_{(\theta_1 + \gamma)} + S_{(\theta_2 - \gamma)}. \quad (35)$$

The remaining relations for each configurations are obtained by following the similar procedure.

4.2. Relation between articular variables and control variables when the SCMS is supported on rear rack and front wheels

The relations for this configuration are shown next:

$$|\mathbf{P}_{C2} - \mathbf{f}(\theta_4)| = |z_2 e^{-j(\delta_2 + \theta_1)} + l_3 (1 + e^{j(\pi - \theta_1 - \theta_2)})| \quad (36)$$

$$\Delta_2 = \arcsin \left(\frac{Im[\mathbf{P}_{C2} - \mathbf{f}(\theta_4)]}{|\mathbf{P}_{C2} - \mathbf{f}(\theta_4)|} \right), \quad (37)$$

$$\gamma = \Delta_2 + \frac{\pi}{2} - \theta_1 - \text{phase} [z_2 e^{-j(\delta_2 + \theta_1)} + l_3 (1 + e^{j(\pi - \theta_1 - \theta_2)})], \quad (38)$$

$$\dot{\gamma} = \frac{-l_3 (S_{(\theta_1 + \gamma)}\dot{\theta}_1 - S_{(\theta_2 - \gamma)}\dot{\theta}_2) + \dot{z}_2 C_{(\delta_2 - \gamma)}}{l_3 (S_{(\theta_1 + \gamma)} + S_{(\theta_2 - \gamma)}) - z_2 S_{(\delta_2 - \gamma)}}, \quad (39)$$

$$\ddot{\gamma} = \frac{num_2}{den_2}, \quad (40)$$

$$num_2 = l_3 [-C_{(\theta_1 + \gamma)}(\dot{\theta}_1 + \dot{\gamma})^2 + C_{(\theta_2 - \gamma)}(\dot{\theta}_2 - \dot{\gamma})^2 + l_3 [-S_{(\theta_1 + \gamma)}\ddot{\theta}_1 + S_{(\theta_2 - \gamma)}\ddot{\theta}_2] + (\ddot{z}_2 - z_2 \dot{\gamma}^2) C_{(\delta_2 - \gamma)} + 2\dot{z}_2 \dot{\gamma} S_{(\delta_2 - \gamma)}], \quad (41)$$

$$den_2 = l_3 (S_{(\theta_1 + \gamma)} + S_{(\theta_2 - \gamma)}) - z_2 S_{(\delta_2 - \gamma)}. \quad (42)$$

4.3. Relation between articular variables and control variables when the SCMS is supported on front rack and rear wheels

The relations for this configuration are illustrated next:

$$|\mathbf{f}(\theta_3) - \mathbf{P}_{C1}| = |z_1 e^{-j(\delta_1 + \theta_1)} - l_3 (1 + e^{j(\pi - \theta_1 - \theta_2)})|, \quad (43)$$

$$\Delta_3 = \arcsin \left(\frac{Im[\mathbf{f}(\theta_3) - \mathbf{P}_{C1}]}{|\mathbf{f}(\theta_3) - \mathbf{P}_{C1}|} \right), \quad (44)$$

$$\gamma = \Delta_3 - \frac{\pi}{2} - \theta_1 - \text{phase} [z_1 e^{-j(\delta_1 + \theta_1)} - l_3 (1 + e^{j(\pi - \theta_1 - \theta_2)})], \quad (45)$$

$$\dot{\gamma} = \frac{-l_3 (S_{(\theta_1 + \gamma)}\dot{\theta}_1 - S_{(\theta_2 - \gamma)}\dot{\theta}_2) - \dot{z}_1 C_{(\delta_1 - \gamma)}}{l_3 (S_{(\theta_1 + \gamma)} + S_{(\theta_2 - \gamma)}) + z_1 S_{(\delta_1 - \gamma)}}, \quad (46)$$

$$\ddot{\gamma} = \frac{num_3}{den_3}, \quad (47)$$

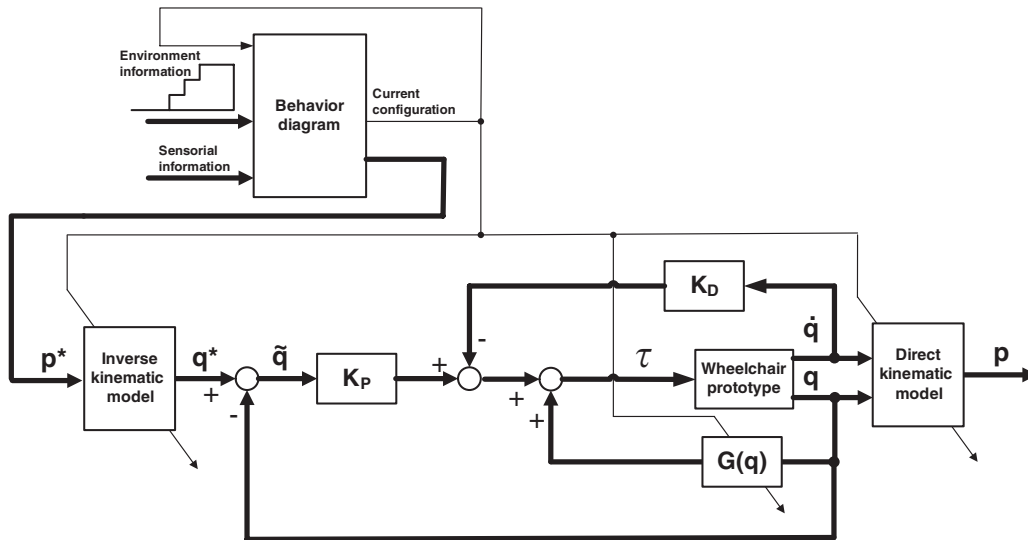


Fig. 5. Control Scheme of the reconfigurable SCMS.

$$\begin{aligned} num_3 &= l_3 [-C_{(\theta_1+\gamma)}(\dot{\theta}_1 + \dot{\gamma})^2 + C_{(\theta_2-\gamma)}(\dot{\theta}_2 - \dot{\gamma})^2] \\ &\quad + l_3 [-S_{(\theta_1+\gamma)}\ddot{\theta}_1 + S_{(\theta_2-\gamma)}\ddot{\theta}_2] \\ &\quad - (\ddot{z}_1 - z_1\dot{\gamma}^2) C_{(\delta_1-\gamma)} + 2\dot{z}_1\dot{\gamma} S_{(\delta_1-\gamma)}, \end{aligned} \quad (48)$$

$$den_3 = l_3 (S_{(\theta_1+\gamma)} + S_{(\theta_2-\gamma)}) + z_1 S_{(\delta_1-\gamma)}. \quad (49)$$

4.4. Relation between articular variables and control variables when the SCMS is supported on both racks
The relations for this configuration are as follows:

$$\Delta_4 = \arcsin \left(\frac{Im [\mathbf{P}_{C2} - \mathbf{P}_{C1}]}{|\mathbf{P}_{C2} - \mathbf{P}_{C1}|} \right), \quad (50)$$

$$\begin{aligned} \gamma &= \Delta_4 - \frac{\pi}{2} - \theta_1 - phase [(z_1 - z_2) e^{-j(\delta+\theta_1)} \\ &\quad + l_3 (1 + e^{j(\pi-\theta_1-\theta_2)})], \\ \dot{\gamma} &= \frac{-l_3 (S_{(\theta_1+\gamma)}\dot{\theta}_1 - S_{(\theta_2-\gamma)}\dot{\theta}_2) - (\dot{z}_1 - \dot{z}_2) C_{(\delta-\gamma)}}{l_3 (S_{(\theta_1+\gamma)} + S_{(\theta_2-\gamma)}) + (z_1 - z_2) S_{(\delta-\gamma)}}, \end{aligned} \quad (51)$$

$$\ddot{\gamma} = \frac{num_4}{den_4}, \quad (52)$$

$$\begin{aligned} num_4 &= -l_3 [C_{(\theta_1+\gamma)}(\dot{\theta}_1 - \dot{\gamma})^2 + C_{(\theta_2-\gamma)}(\dot{\theta}_2 - \dot{\gamma})^2] \\ &\quad - l_3 [S_{(\theta_1+\gamma)}\ddot{\theta}_1 - S_{(\theta_2-\gamma)}\ddot{\theta}_2] \\ &\quad - 2(\dot{z}_1 - \dot{z}_2)\dot{\gamma} S_{(\delta_1-\gamma)} \\ &\quad - (\ddot{z}_1 - \ddot{z}_2 + (z_1 - z_2)\dot{\gamma}^2) C_{(\delta-\gamma)}, \end{aligned} \quad (53)$$

$$den_4 = l_3 (S_{(\theta_1+\gamma)} + S_{(\theta_2-\gamma)}) + (z_1 - z_2) S_{(\delta-\gamma)}. \quad (54)$$

5. Control Scheme

With regard to the mechanical structure, modularity was a key factor in the system design. The SCMS-driven degrees of freedom are split into two categories: the first concerning the locomotion itself (traction and step ascent), and the second

concerning the position and verticality of the chair frame. Both categories will be dealt with together in the control scheme.

The objective of the control scheme is to obtain an accurate robot posture. This achievement implies improvement in passenger comfort when it is evaluated as a reduction of vibrations and accelerations of SCMS during the climbing/descent process. For this purpose, the control architecture of the system has been decomposed into several modules. Each individual module is in charge of carrying out one particular job that corresponds with different configurations (or behaviors) of SCMS that may appear during the climbing/descent process. This approach is a vertical decomposition of navigation problem and behaves correctly in dynamic environments in which the knowledge of the terrain is not perfectly known.²⁰ At each instant of navigation, the control architecture of the SCMS prototype extracts the sensor information (ultrasounds and wheel-switches) from the local robot environment. Under certain sensor values, the corresponding transition between two configurations is achieved, and then the controller activates appropriate behavior, which provides the center of mass trajectories and the null inclination of the chair frame ($\mathbf{p}^* = [x^*, y^*, \gamma^* = 0]^T$). The inverse kinematic model presented in ref. [15] allows us to obtain reference trajectories in charge of the movement of the actuated degrees of freedom ($\mathbf{q}^* = [\theta_1^*, \theta_2^*, \theta_3^*, z_1^*, z_2^*]^T$) of SCMS in each possible configuration. Then a control system is used to control the posture of the SCMS prototype. Taking advantage of the excellent properties of the proposed mechanical design, the control system of the prototype will be divided into two different parts: (a) selection of appropriate SCMS configuration; and (b) design of a feedback control law for each SCMS configuration to maintain passenger comfort and control posture of SCMS. Figure 5 illustrates the general control scheme of the SCMS prototype, and a detailed description of each part of the control system will be explained in the following subsections.

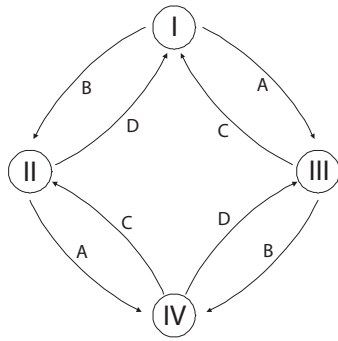


Fig. 6. Behavior diagram of the reconfigurable SCMS.

5.1. Selection of SCMS configuration

In order to solve the selection of appropriate SCMS configuration, based on the knowledge of current configuration and information that comes from the sensor system (see Fig. 5), a *behavior diagram* has been developed, which is depicted in Fig. 6. This diagram greatly helps to understand transitions of the prototype from one configuration to the next when the SCMS is working to overcome an architectural barrier. The diagram is similar to an addressed state-transition diagram with additional information. The nodes show different prototype behaviors or configurations and are used to point out the current behavior of the SCMS prototype. The diagram arrows are behavior transitions. If one of the transitions from the current state is activated, the current behavior will change to a new behavior, which is pointed out by the end of the transition arrow. Finally, meanings of all behaviors and all transitions that appear during the climbing/descent process (see Fig. 6) are defined as follows:

1. *Behaviors*: These correspond to different SCMS configurations that may appear during the staircase climbing/descent process.
 - I. SCMS supported on four wheels.
 - II. SCMS supported on rear rack and front wheels.
 - III. SCMS supported on front rack and rear wheels.
 - IV. SCMS supported on both racks.
2. *Transitions*: The information that comes from the internal sensorial system (switches that indicate the end position of wheels) and the external sensorial system (ultrasound sensors).
 - A. The distance between the front wheel axle and the step is lower than a predefined threshold.
 - B. The distance between the rear wheel axle and the step is lower than a predefined threshold.
 - C. Front wheels completely overcome the obstacle.
 - D. Rear wheels completely overcome the obstacle.

5.2. Design of a nonlinear feedback controller

In order to follow a methodological approach that is consistent with control design, it is necessary to treat the control problem in the context of nonlinear multivariable systems. This approach will obviously account for the SCMS dynamics model and lead to find a nonlinear centralized control law, whose implementation is needed for a better prototype dynamic performance. In our particular case, to fulfil the passenger comfort requirements, the SCMS has

to move at very low velocities ($\|\dot{\mathbf{q}}\| \leq c$ with c small) and the control of the posture of the SCMS can be solved using static principles.²¹ For this reason, a control law based on PD linear action and nonlinear gravity compensation term has been designed. Defining \mathbf{q}^* as the vector of desired joint variables, $\tilde{\mathbf{q}} = \mathbf{q}^* - \mathbf{q}$ represents the error between the desired and the actual posture, $[\tilde{\mathbf{q}}^T \dot{\tilde{\mathbf{q}}}^T]^T$ is defined as the system state, and \mathbf{K}_P and \mathbf{K}_D are $(n \times n)$ diagonal and positive definite matrix of the PD linear controller, and the input control $\boldsymbol{\tau}$ that stabilizes the system around equilibrium posture is given by the following expression:

$$\boldsymbol{\tau} = \mathbf{G}(\mathbf{q}) + \mathbf{K}_P \tilde{\mathbf{q}} - \mathbf{K}_D \dot{\tilde{\mathbf{q}}}. \tag{55}$$

Remark. Let a constant equilibrium posture be assigned for the system as the vector of desired joint variables \mathbf{q}^* . It is desired to find the structure of the controller that ensures global asymptotic stability of the above posture. The determination of the control input that stabilizes the system around the equilibrium posture is based on the Lyapunov control theory. We define vector $[\tilde{\mathbf{q}}^T \dot{\tilde{\mathbf{q}}}^T]^T$ as the system state, where $\tilde{\mathbf{q}} = \mathbf{q}^* - \mathbf{q}$ represents the error between the desired and the actual postures, and we choose the following positive definite quadratic form as the Lyapunov function candidate:

$$V(\tilde{\mathbf{q}}, \dot{\tilde{\mathbf{q}}}) = \frac{1}{2} \dot{\tilde{\mathbf{q}}}^T \mathbf{B}(\mathbf{q}) \dot{\tilde{\mathbf{q}}} + \frac{1}{2} \tilde{\mathbf{q}}^T \mathbf{K}_P \tilde{\mathbf{q}} > 0, \forall \tilde{\mathbf{q}}, \dot{\tilde{\mathbf{q}}} \neq \mathbf{0}. \tag{56}$$

An energy-based interpretation of Eq. (56) reveals that the first term expresses the system kinetic energy ($\mathbf{B}(\mathbf{q})$ is symmetric and positive definite matrix) and the second term expresses the potential energy stored in the system of equivalent stiffness \mathbf{K}_P provided by the n position feedback loops. A plausible policy to attain the desired condition, $\tilde{\mathbf{q}} \equiv \mathbf{0}$, is to adopt action for the control input $\boldsymbol{\tau}$, which results in a strict decrease of function $V(\tilde{\mathbf{q}}, \dot{\tilde{\mathbf{q}}})$. This can be achieved by influencing the system in such a manner that the speed of variation of $V(\tilde{\mathbf{q}}, \dot{\tilde{\mathbf{q}}})$ will be strictly negative. In other words,

$$\frac{d}{dt} V(\tilde{\mathbf{q}}, \dot{\tilde{\mathbf{q}}}) < 0. \tag{57}$$

By differentiating Eq. (56) and recalling that \mathbf{q}^* is constant, yields

$$\dot{V} = \dot{\tilde{\mathbf{q}}}^T \mathbf{B}(\mathbf{q}) \dot{\tilde{\mathbf{q}}} + \frac{1}{2} \dot{\tilde{\mathbf{q}}}^T \dot{\mathbf{B}}(\mathbf{q}) \dot{\tilde{\mathbf{q}}} - \dot{\tilde{\mathbf{q}}}^T \mathbf{K}_P \tilde{\mathbf{q}}. \tag{58}$$

Solving Eq. (23) for $\mathbf{B}(\mathbf{q}) \cdot \dot{\tilde{\mathbf{q}}}$ and substituting it in Eq. (56) gives

$$\dot{V} = \frac{1}{2} \dot{\tilde{\mathbf{q}}}^T (\dot{\mathbf{B}}(\mathbf{q}) - 2\mathbf{C}(\mathbf{q}, \dot{\mathbf{q}})) \dot{\tilde{\mathbf{q}}} + \dot{\tilde{\mathbf{q}}}^T (\boldsymbol{\tau} - \mathbf{G}(\mathbf{q}) - \mathbf{K}_P \tilde{\mathbf{q}}). \tag{59}$$

The first term on the right-hand side is null, since the matrix $\mathbf{N} = \dot{\mathbf{B}} - 2\mathbf{C}$ is a *skew-matrix*²² and satisfies the property $\mathbf{w}^T \mathbf{N}(\mathbf{q}, \dot{\mathbf{q}}) \mathbf{w} = 0$ for any vector $\mathbf{w}_{n \times 1}$. The second term is negative-definite diagonal matrix, assuming perfect cancelation of terms and using in Eq. (59) the following

Table I. Some prototype specifications.

Max. passenger weight	100 kg
Vehicle plus battery weight	40 + 50 kg = 90 kg
Power source (battery)	12 V 56 AH x 2
Operating range (time)	
Barrier free operation	6.4 h
Stair operation	3.7 h
Stair-climbing speed (max.)	3 steps per min.
Speed on the flat (max.)	2 km/h
Max. height step	215 mm
Max. slope allowable	45°
Angle of the climbing mechanisms (δ_1 and δ_2)	35°

control input choice,

$$\tau = \mathbf{G}(\mathbf{q}) + \mathbf{K}_P \tilde{\mathbf{q}} - \mathbf{K}_D \dot{\tilde{\mathbf{q}}}, \quad (60)$$

which corresponds to a nonlinear compensation action of gravitational term, $\mathbf{G}(\mathbf{q})$, with a linear PD action. In fact, substituting Eq. (60) into Eq. (59) gives

$$\dot{V} = -\dot{\tilde{\mathbf{q}}}^T \mathbf{K}_D \dot{\tilde{\mathbf{q}}}, \quad (61)$$

which, in accordance with Eq. (57) and the function candidate V , decreases as long as $\dot{\tilde{\mathbf{q}}} \neq \mathbf{0}$ for all system trajectories. It can be shown that the system reaches an equilibrium posture. To find such a posture, note that $\dot{V} \equiv 0$ only if $\dot{\tilde{\mathbf{q}}} \equiv \mathbf{0}$. The system dynamics under nominal control (60) is given by

$$\mathbf{B}(\mathbf{q})\ddot{\mathbf{q}} + \mathbf{C}(\mathbf{q}, \dot{\mathbf{q}})\dot{\mathbf{q}} + \mathbf{G}(\mathbf{q}) = \mathbf{G}(\mathbf{q}) + \mathbf{K}_P \tilde{\mathbf{q}} - \mathbf{K}_D \dot{\tilde{\mathbf{q}}}. \quad (62)$$

At the equilibrium ($\dot{\mathbf{q}} \equiv \mathbf{0}$, $\ddot{\mathbf{q}} \equiv \mathbf{0}$) it is

$$\mathbf{K}_P \tilde{\mathbf{q}} = \mathbf{0}, \quad (63)$$

and then

$$\tilde{\mathbf{q}} = \mathbf{q}^* - \mathbf{q} \equiv \mathbf{0} \quad (64)$$

in the sought equilibrium posture. The above derivation rigorously shows that the SCMS equilibrium posture is globally asymptotically stable under a controller with a PD linear action and a nonlinear gravity compensating action. Stability is ensured for any choice of \mathbf{K}_P and \mathbf{K}_D as long as these are positive definite matrices. The resulting control block was shown in Fig. 5. Finally, we have to note that the control law requires the on-line computation of term $\mathbf{G}(\mathbf{q})$, and the case of a non-perfect gravity term compensation will be arranged in Section 6.

6. Experimental Results

In this section, the experimental results performed to validate the dynamic control of the SCMS prototype are described. The geometrical parameters, the working environment, and some specifications of the real prototype are illustrated in Fig. 7 and Table I. Upon study Table I, it is noted that the speed in flat mode (SCMS supported on wheels) is slower than commercial EPWs. The reason for this is that the purpose of this first prototype was to overpass architectural barriers. All the motors were therefore selected with high gearheads.

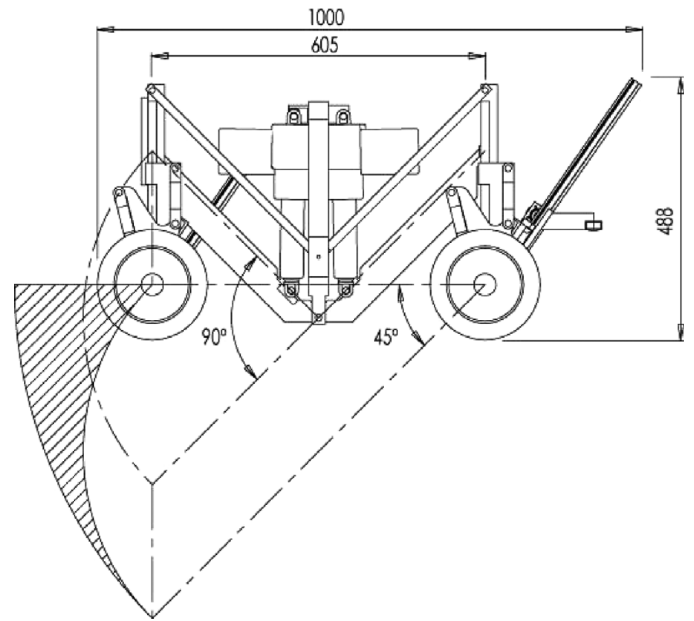


Fig. 7. Geometrical parameters and work environment (dimensions in mm).

At present, this has been obtained by a complete knowledge of different requirements, and the value of gearheads of the wheel drive motors could be reduced without collateral problems in the rest of the system. The same power consumption can thus be maintained while the velocity is increased. In order to verify the SCMS control system validation, the real prototype behavior is studied while it climbs a three-step staircase. The considered step dimensions are 180 mm (height) and 300 mm (width). In all the experiments, the mass m is known, and the profile trajectory of the center of mass (\mathbf{P}_g) of the prototype consists of straight lines with the same slope as the racks (when the SCMS is in a mixed configuration or supported on both racks) or horizontal lines (when the SCMS is supported on wheels). This particular profile was chosen because the control system is substantially simplified and the power consumption is decreased (see ref. [18]). Furthermore, the movements had to satisfy the following three conditions: (a) Maintain the seat inclination; (b) accurate tracking trajectory of the center of mass; and (c) maintenance of passenger comfort. This third constraint implies that the movement of the SCMS will consist of two stages – one to accelerate the SCMS, and the other to decelerate it. More information about comfort trajectories of the SCMS can be found in ref. [23].

The experimental results have been split into two modules: (a) Climbing a staircase using a PD control scheme without compensation of gravitational terms; and (b) climbing a staircase using a PD control with the addition of a nonlinear compensation of gravitational terms. Taking into account all previous considerations, the results obtained using the real prototype are described next.

6.1. Control of SCMS using a PD control without compensation of gravitational terms

Figures 8 and 9 illustrate the evolution of total articular torques, τ_1 and τ_2 , when the SCMS climbs a staircase

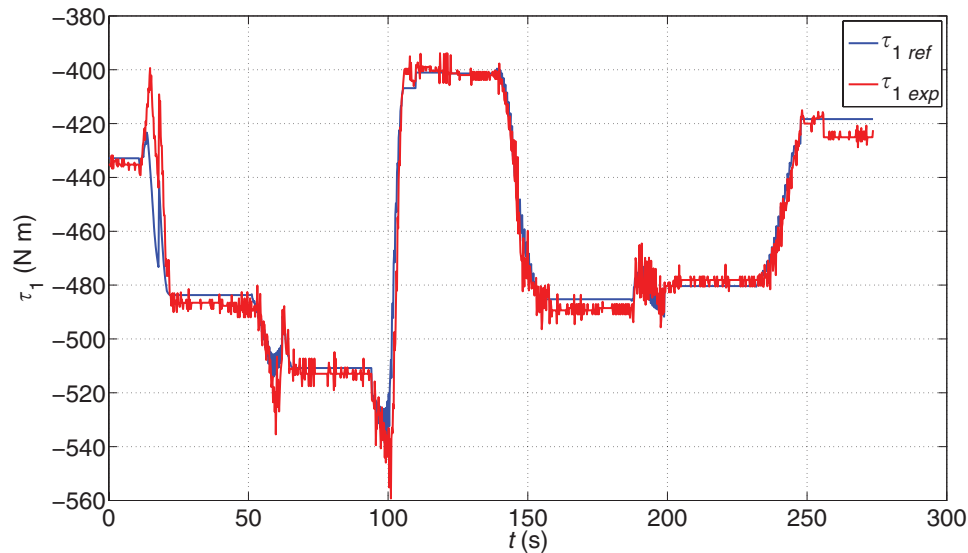


Fig. 8. (Colour online) Evolution of total articular torque τ_1 when the SCMS climbs a staircase using a PD control without compensation of gravitational terms.

using a PD control without compensation of gravitational terms. Note that a constant error between theoretical and experimental trajectories of total articular torques, τ_1 and τ_2 , appears during all the experiment. This error can be computed by means of the control system analysis explained in Section 5. Considering that the gravity compensation term is not used, the achievement of the equilibrium posture ($\dot{\mathbf{q}} \equiv \mathbf{0}$ and $\ddot{\mathbf{q}} \equiv \mathbf{0}$) gives a small error between the desired and the actual posture $\tilde{\mathbf{q}}$ that is modeled as

$$\tilde{\mathbf{q}} = \mathbf{K}_P^{-1} \mathbf{G}(\mathbf{q}) = \mathbf{K}_P^{-1} \mathbf{J}^T \mathbf{g}, \quad (65)$$

where $\mathbf{G}(\mathbf{q}) = \mathbf{J}^T \mathbf{g}$, \mathbf{g} is the gravity acceleration, \mathbf{J} is the geometric Jacobian in terms of system variables, and the matrices \mathbf{K}_P and \mathbf{K}_D have been designed to obtain the fastest possible response without any overshooting and saturation

Table II. Gain matrix of the control scheme.

$\mathbf{K}_P = \text{diag}(257.5631, 257.5593, 258.4746, 258.4833, 258.4805)$
$\mathbf{K}_D = \text{diag}(7.644, 7.683, 8.632, 8.691, 8.602)$

(under small amplitude step signal inputs). Table II illustrates the real values used in the experimental platform. The obtained high values of matrix \mathbf{K}_P ensures very small errors according to Eq. (65). Considering that the values of \mathbf{J} are fenced, and the fact that the diagonal definite positive matrix \mathbf{K}_P has been designed with high gain values (see Table II), upon substituting values in Eq. (65) a small value of $\|\tilde{\mathbf{q}}\| \approx 0.05$ [rad] is achieved. In the following section, the magnitude of error $\tilde{\mathbf{q}}$ will be reduced by adding the nonlinear compensation of gravitational terms into the control scheme.

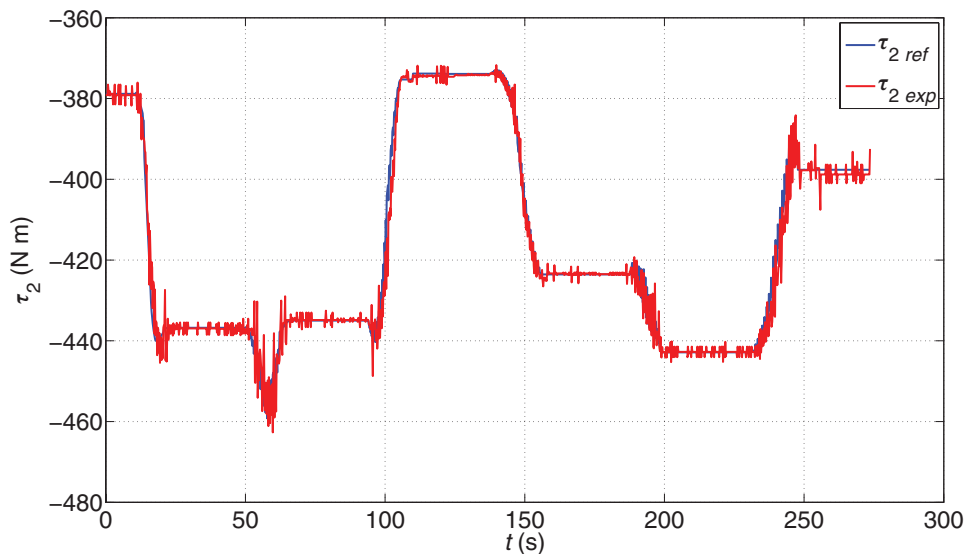


Fig. 9. (Colour online) Evolution of total articular torque τ_2 when the SCMS climbs a staircase using a PD control without compensation of gravitational terms.

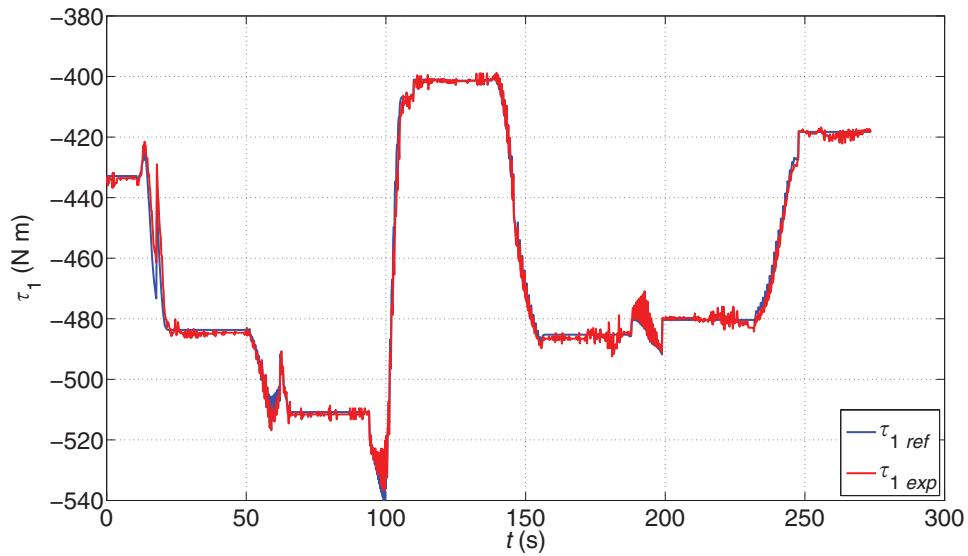


Fig. 10. (Colour online) Evolution of total articular torque τ_1 when the SCMS climbs a staircase using a PD control with compensation of gravitational terms.

6.2. Control of SCMS using a PD control with nonlinear gravitational compensation terms

By using the compensation of gravitational terms in the control law (see Fig. 5) the error value between the desired and the actual posture ($\tilde{\mathbf{q}}$) is reduced substantially. To demonstrate the effect of the addition of the gravity compensation term in the control law, the on-line computation of the matrix $\mathbf{G}(\mathbf{q})$ are carried out (obtained) from

$$\hat{\mathbf{G}}(\mathbf{q}) = \mathbf{J}^T(\hat{g}), \tag{66}$$

where \hat{g} is the estimation of the gravity acceleration. Now assuming that the system dynamics is under control, it can be found that at equilibrium ($\dot{\mathbf{q}} \equiv \mathbf{0}, \ddot{\mathbf{q}} \equiv \mathbf{0}$) the error $\tilde{\mathbf{q}}$ is expressed by the following expression:

$$\tilde{\mathbf{q}} = \mathbf{K}_p^{-1} [\mathbf{G}(\mathbf{q}) - \hat{\mathbf{G}}(\mathbf{q})] = \mathbf{K}_p^{-1} \mathbf{J}^T(g - \hat{g}). \tag{67}$$

Note that the minimum error between theoretical and experimental trajectories of total articular torques, τ_1 and τ_2 , occurred when the estimation of gravitational terms coincide with real gravitational terms of the prototype. The desired equilibrium posture $\tilde{\mathbf{q}} \equiv \mathbf{0}$ is thus obtained with very small errors, thanks to the computation of an accurately on-line estimation of term $\hat{\mathbf{G}}(\mathbf{q})$. The experimental results reported illustrate that the addition of the nonlinear gravitational compensation term $\hat{\mathbf{G}}(\mathbf{q})$ into the control scheme improves the obtention of equilibrium posture. Figures 10 and 11 depict the evolution of the total articular torques (τ_1 and τ_2) when the SCMS climbs a staircase using a PD control with compensation of gravitational terms. In order to show a quantitative comparison between the trajectories of total articular torques with and without gravity compensation, evolution of relative error of total articular torques has been included. Figures 12 and 13 illustrate the achieved results. It is observed that the agreement between reference and

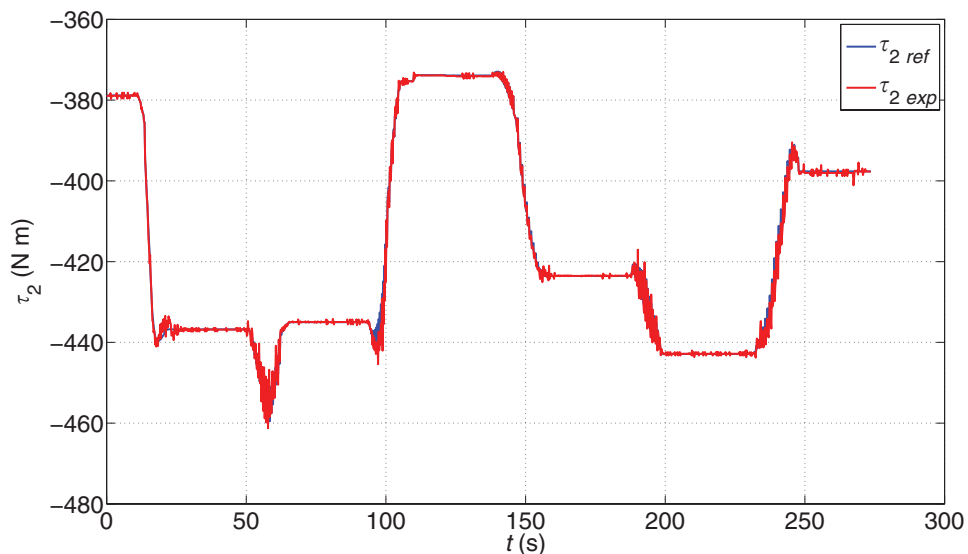


Fig. 11. (Colour online) Evolution of total articular torque τ_2 when the SCMS climbs a staircase using a PD control with compensation of gravitational terms.

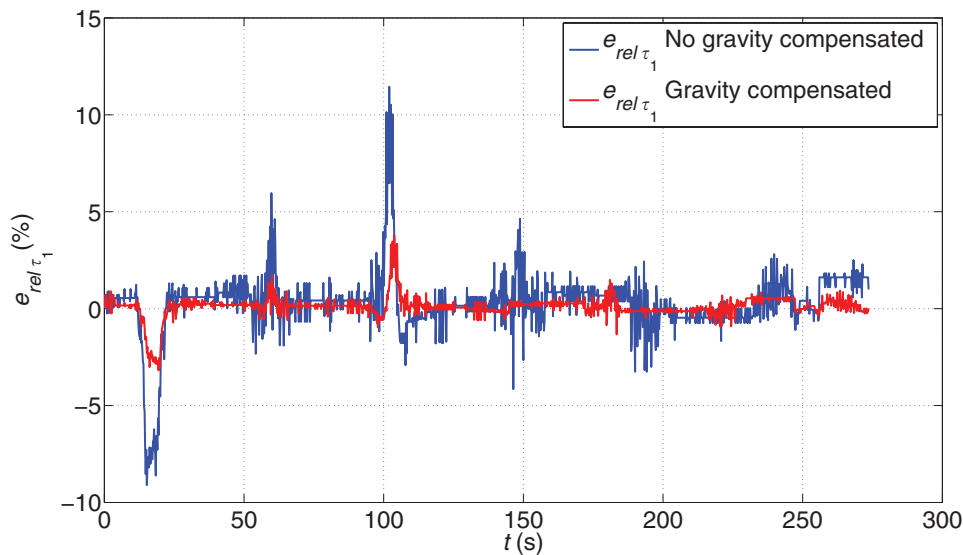


Fig. 12. (Colour online) Evolution of relative error of the total articular torque $e_{rel\tau_1}$ when the SCMS climbs a staircase using a PD control with and without compensation of gravitational terms.

experimental trajectories of both variables (in both experiments) is very good, giving small relative error values of total articular torques. Moreover, Figures 12 and 13 depict better behavior of the prototype when the SCMS is controlled by using the compensation of gravitational terms. A direct consequence of the improvement obtained in the tracking trajectory of the desired posture is a benefit for tracking evolution of the center of mass and therefore in passenger comfort. On the one hand, Fig. 14 illustrates the evolution of the center of mass trajectory using both control algorithms. A smoother and a more accurate tracking evolution is observed when the SCMS implements the algorithm with compensation of gravitational terms. On the other hand, to study the problem of comfortability, it has used the criteria developed in ref. [24]. Basically, the criteria evaluates the tolerance of the human body when it is exposed to vibrations, and interprets the existent data. In a particular case

of SCMSs, depending on passenger position, the vibrations could be transmitted to feet, behind, or back. The criteria measures the vibration intensity as root mean square (rms) of acceleration. If the peak factor (relation between maximum acceleration and vibration intensity) is less than 1, the system is in a situation of ideal comfort intervals. When the peak factor is less than 1, passenger comfort begins to decrease. Peak factor values that are more than 1 and less than 3 imply acceptable vibration tolerance values and acceptable comfort values. Finally, peak factor values of more than 6 imply that the maximum limit of tolerance vibration has surpassed, and damage to passenger start to appear. The estimation of vibration intensity value (rms) was selected according to ref. [25] and is approximately 2.5 m/s^2 . A comfortability comparison between both versions of control algorithm is depicted in Fig. 15. The comfortability values are maintained within comfortability margins throughout the experiments

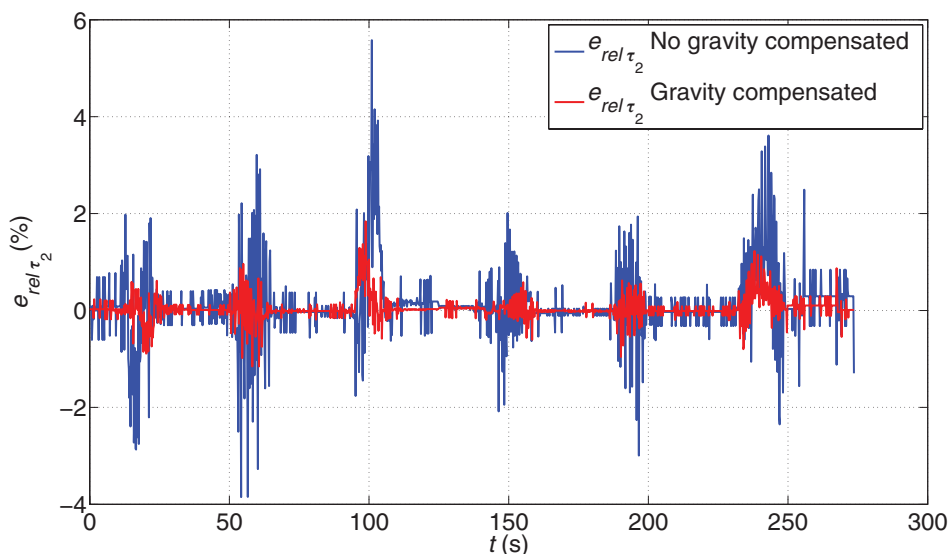


Fig. 13. (Colour online) Evolution of relative error of the total articular torque $e_{rel\tau_2}$ when the SCMS climbs a staircase using a PD control with and without compensation of gravitational terms.

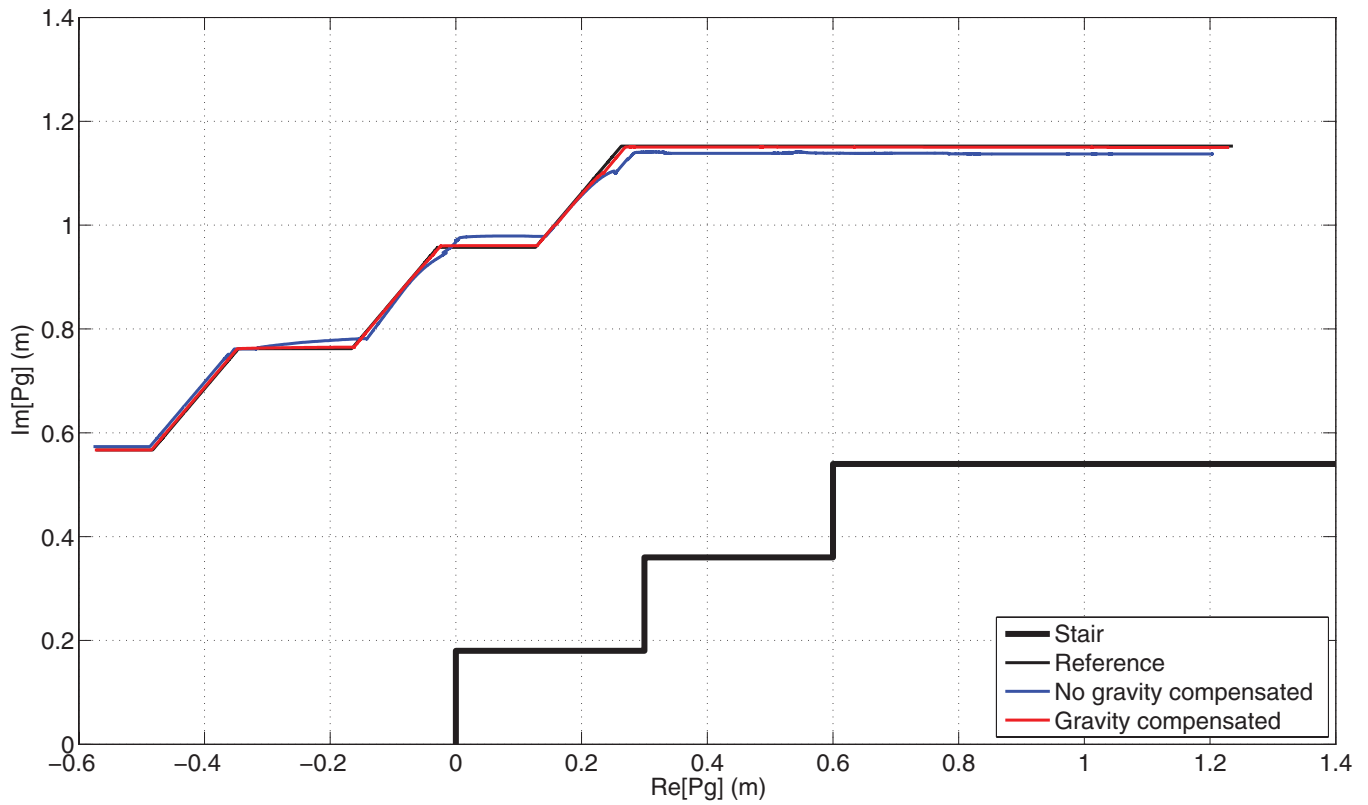


Fig. 14. (Colour online) Trajectory evolution of the center of mass when the SCMS climbs a staircase using a PD control with and without compensation of gravitational terms.

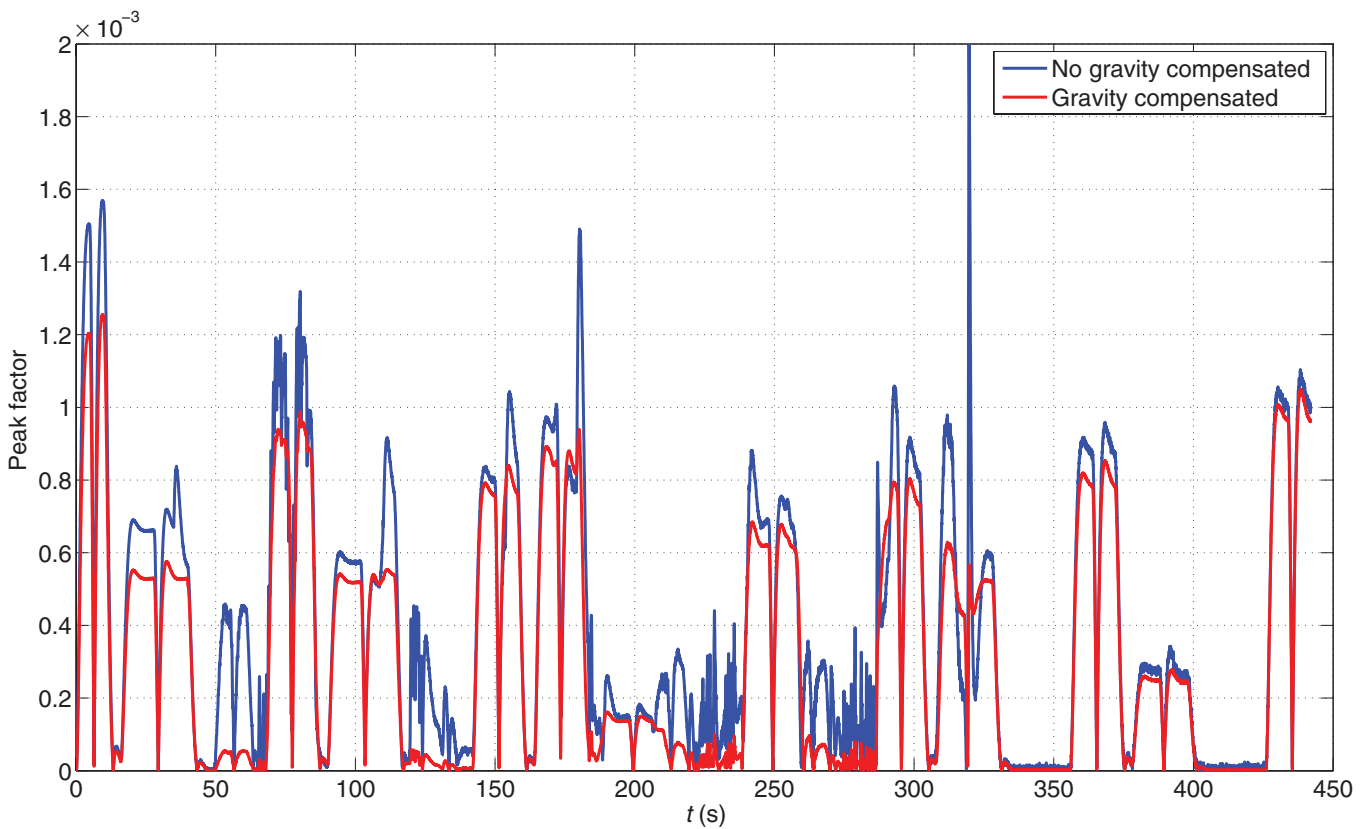


Fig. 15. (Colour online) Peak factor evolution of the center of mass when the SCMS climbs a staircase using a PD control with and without compensation of gravitational terms.

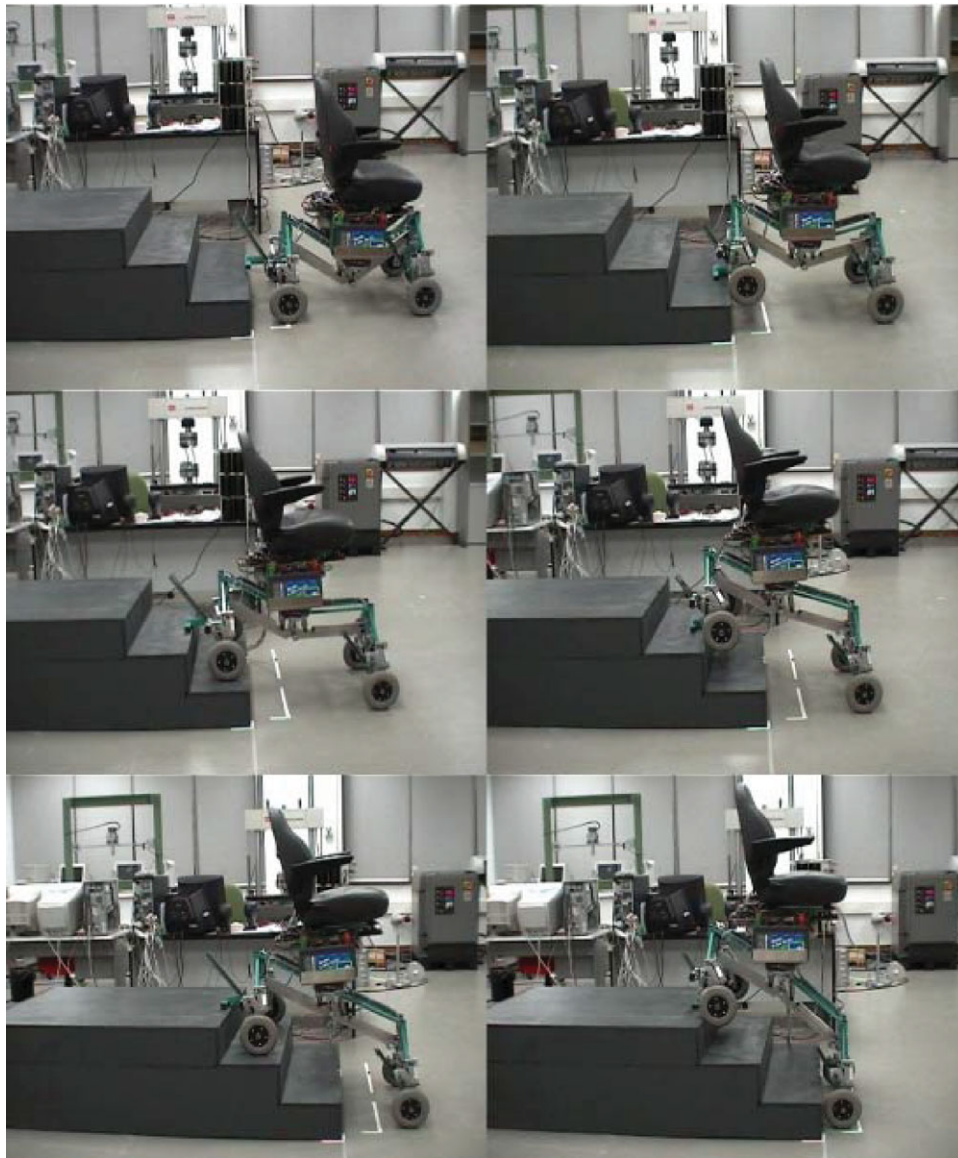


Fig. 16. (Colour online) Sequence of a climbing process (part A).

in both cases. However, the peak factor values when using the control algorithm without gravity compensation are slightly higher, which demonstrates that the use of control algorithm with compensation of gravitational terms reports increase of comfortability. Finally, a visual sequence of the climbing process is illustrated in Figs. 16 and 17, showing different configurations of SCMS and maintenance of seat's verticality.

7. Conclusions

In order to obtain a successful stair-climbing process, an improvement to passenger comfort, and an accurate robot posture, it is necessary to incorporate the dynamics model within the feedback control law. A high reliability between model-experiment has been obtained by using a control system based on the SCMS transition diagram and a linear PD action with a nonlinear compensation of gravitational terms. These control schemes have had a widespread use in several commercial industrial robots, but it has seldom been

used on SCMS. The planned trajectories were consistent and agreed with experimental results, and illustrate an accurate tracking of the desired posture of a robotized system by the incorporation of nonlinear gravity term within the control law. The tests demonstrated that the SCMS design is capable to climb stairs while guaranteeing stability and passenger comfort. Moreover, the proposed control scheme and the compensation of gravitational terms improved the behavior of SCMS as (a) response to perturbations in the system, error modeling, and environmental uncertainties; (b) better steady state response; (c) improvement of passenger comfort and achievement of smoother configuration changes; and (d) adaptation of gravity compensation, $\mathbf{G}(\mathbf{q})$, is immediately computed when the mass of the passenger is known, and this can be obtained when a sensorial system detects a passenger on the prototype. Finally, an additional advantage is that the method implemented in this work demonstrates that it is a simple control strategy, computationally efficient, and easily implementable in a microprocessor-/microcontroller-based system.

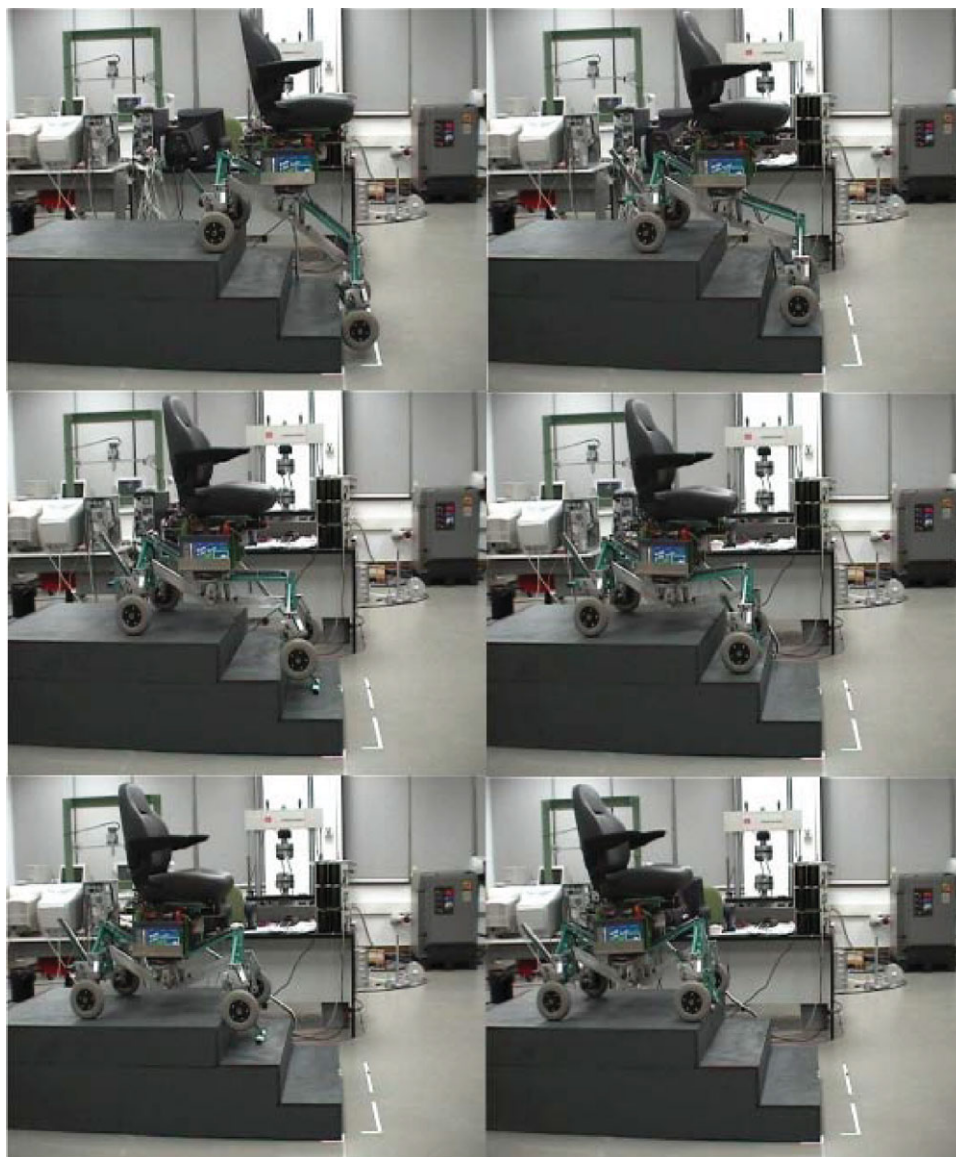


Fig. 17. (Colour online) Sequence of a climbing process (part B).

In future work, based on more than satisfactory results obtained in this research, different experimental branches are the focus of our attention. They are detailed as follows: (a) Improve the design of climbing mechanisms to reduce the prototype's geometry and obtain a system that is capable of confronting obstacles with more varied geometries; and (b) study different control strategies and new trajectory generations, taking advantage of additional degrees of freedom of positioning mechanisms to increase the level of passenger comfort.

Acknowledgments

This work has been partially supported by Spanish Research Grant DPI2011-24113.

References

1. A. B. Wilson Jr., *Wheelchairs: A Prescription Guide*, 2nd ed. (Demos, New York, NY, 1992).
2. R. A. Cooper, *Wheelchairs Selection and Configuration* (Demos Medical, New York, 1998).
3. D. Ding, R. A. Cooper, S. Terashima, Y. S. Yang and R. Cooper, "A Study on the Balance Function of the iBOT Transporter," *Proceedings of the RESNA 2004 Annual Conference*, Orlando, FL, USA (2004).
4. C. Rados, "FDA works to reduce preventable medical device injuries," *FDA Consum.* **37**(4), 29–33 (2003).
5. Sunwa Co. Ltd., *Sunwa Stair-Ship TRE-52* (Sendagaya, Shiuya-ku, Tokyo, Japan). available at: <http://www.sunwa-jp.co.jp> (2012).
6. M. J. Lawn and T. Ishimatzu, "Modelling a stair-climbing wheelchair mechanism with high single-step capability," *IEEE Trans. Neural Syst. Rehabil. Res.* **11**(3), 323–332 (2003).
7. S. Hirose, "A study of design and control of a quadruped walking vehicle," *Int. J. Robot. Res.* **3**(2), 113–133 (1984).
8. S. Hirose and H. Takeuchi, "Study on roller-walk (basic characteristics and its control)," *In: Proceedings of the IEEE International Conference on Robotics and Automation*, Minneapolis, MN, USA (Apr. 1996) pp. 3265–3270.
9. P. Wellman and V. Krovi, "Design of a wheelchair with legs for people with motor disabilities," *IEEE Trans. Rehabil. Eng.* **3**(4), 343–353 (1995).
10. D. Pavec, C. E. Aubin, R. Aissaoui, F. Parent and J. Dansereau, "Kinematic modeling for the assesment of wheelchair user's stability," *IEEE Trans. Neural Syst. Rehabil. Eng.* **9**(4), 362–368 (2001).

11. J. D. Yoder, E. T. Baumgartner and S. B. Skaar, "Initial results in the development of a guidance system for a powered wheelchair," *IEEE Trans. Rehabil. Eng.* **4**(3), 143–151 (1996).
12. D. Ding, R. A. Cooper, S. Guo and T. A. Corfman, "Analysis of driving backward in an electric-powered wheelchair," *IEEE Trans. Control Syst. Technol.* **12**(6), 934–943 (2004).
13. Y. Takahashi, S. Ogawa and S. Machida, "Mechanical design and control system of robotic wheelchair with inverse pendulum control," *Trans. Inst. Meas. Control* **24**(5), 355–368 (2002).
14. A. González, R. Morales, V. Feliu and P. Pintado, "Improving the mechanical design of new staircase climbing wheelchair," *Ind. Robot Int. J.* **34**(2), 110–115 (2007).
15. R. Morales, V. Feliu, A. González and P. Pintado, "Kinematic model of a new staircase climbing wheelchair and its experimental validation," *Int. J. Robot. Res.* **25**(9), 825–841 (2006).
16. V. Feliu, J. A. Somolinos and A. Garcia, "Inverse dynamics-based control system for a three degree-of-freedom flexible arm," *IEEE Trans. Robot. Autom.* **19**(6), 1007–1014 (2003).
17. J. A. Somolinos, V. Feliu and A. Garcia, "Stability Analysis of a New Control Scheme for a Three-Degree-of-Freedom Flexible Robot," *In: Proceedings of the IEEE-CSS 39th International Conference on Decision and Control*, Sydney, Australia (Dec. 2000) pp. 4030–4035.
18. R. Morales, A. González, V. Feliu and P. Pintado, "Environment adaptation of a new staircase climbing wheelchair," *Auton. Robots* **23**, 275–292 (2007).
19. R. Morales, J. A. Somolinos and J. A. Cerrada, "Dynamic model of a stair-climbing mobility system and its experimental validation," *Multibody Syst. Dyn.* (2012) doi: 10.1007/s11044-012-9310-2.
20. R. Arkin, "Motor schema-based mobile robot navigation," *Int. J. Robot. Res.* **8**, 92–112 (1989).
21. L. Sciavicco and B. Siciliano, *Modelling and Control of Robot Manipulators*, 2nd ed. (Springer, Berlin, Germany, 2000).
22. J. J. Craig, *Introduction to Robotics – Mechanics and Control*, 3rd ed. (Addison-Wesley Longman, Indianapolis, IN, 2008).
23. R. Morales, V. Feliu, A. González and P. Pintado, "Coordinated Motion of a New Staircase Climbing Wheelchair With Increased Passenger Comfort," *In: Proceedings of the 2006 IEEE International Conference on Robotics and Automation*, Orlando, FL, USA (2006) pp. 3395–4001.
24. R. Morales, V. Feliu and A. González, "Optimized obstacle avoidance trajectory generation for a reconfigurable staircase-climbing wheelchair," *Robot. Auton. Syst.* **58**, 97–114 (2010).
25. P. Pintado, "Un Curso de Automoción," (Sección de Publicaciones Área de Ingeniería Mecánica, Universidad de Castilla-La Mancha, Spain, 1994).